

# Graphene Quantum Dot with Divacancy and Topological Defects: A Novel Material for Promoting Prompt and Delayed Fluorescence of Tunable Wavelengths

Tushima Basak,<sup>\*,†</sup> Tista Basak,<sup>\*,‡</sup> and Alok Shukla<sup>\*,¶</sup>

<sup>†</sup>*Department of Physics, SVKM's Mithibai College of Arts Chauhan Institute of Science & Amrutben Jivanlal College of Commerce and Economics, Mumbai 400056, India*

<sup>‡</sup>*Mukesh Patel School of Technology Management and Engineering, NMIMS University, Mumbai 400056, India*

<sup>¶</sup>*Department of Physics, Indian Institute of Technology Bombay, Powai, Mumbai 400076, India*

E-mail: Tushima.Basak@mithibai.ac.in; tista.basak@nmims.edu; shukla@phy.iitb.ac.in

## Abstract

This work demonstrates the unique approach of introducing divacancy imperfections in topological Stone-Wales type defected graphene quantum dots for harvesting both singlet and triplet excitons, essential for fabricating fluorescent organic light-emitting diodes. Here, we first reveal that structural relaxation of these systems establishes the high-spin triplet state as the stable ground state at room temperature, thereby significantly increasing their potential in designing spintronic devices. Our extensive electron-correlated computations then demonstrate that the energetic ordering of the singlet and triplet states in these relaxed structures can trigger both prompt and delayed

fluorescence of different wavelengths through various decay channels. Particularly, the position of divacancy determines the tunability range of the emission wavelengths. In addition, our results obtained from both multi-reference singles-doubles configuration-interaction (MRSDCI) and first-principles time-dependent density functional theory (TDDFT) methodologies highlight that the synergetic effects of divacancy-position, structural relaxation and spin multiplicity critically govern the nature and magnitude of shift exhibited by the most intense peak of the absorption profile, crucial for designing optoelectronic devices.

## Introduction

The development of unique materials with tunable electronic and optical properties, required for optimizing the performance of optoelectronic devices, has been a crucial theoretical and technical challenge in recent years<sup>1</sup>. In principle, high optical efficiency can be achieved in these new-generation materials by the simultaneous harvesting of singlet and triplet excitons. In this work, we propose for the first time, an efficient mechanism of exploiting the structural relaxation process associated with the suitable incorporation of divacancy and Stone-Wales (SW) type topological defects in graphene quantum dots (GQDs) for promoting both prompt and delayed fluorescence of varied wavelengths, which is crucial for designing fluorescent organic light-emitting diodes (FOLEDs).

The formation and reconstruction of *in situ* atomic point defects (single vacancy and double vacancy) and topological anomalies like SW-type bond reconstructions, created ubiquitously during facile synthesis of graphene, has been precisely imaged by atomic resolution microscopy techniques like scanning tunneling microscopy (STM) and aberration corrected transmission electron microscopy (ac-TEM)<sup>2,3</sup>. In particular, TEM measurements<sup>4</sup> have demonstrated that double vacancies (DVs) are more abundant than single vacancies (SVs) at room temperature. Further, ac-TEM measurements<sup>5</sup> have recorded the real-time evolution of DVs in graphene into different SW-type bond reconstructed patterns such as triple

pentagon-triple heptagon (555-777) and pentagon-octagon-pentagon (5-8-5) configurations within a time-scale of few seconds.

Theoretical studies have also affirmed the relative stability of various types of DV reconstructed structures<sup>6</sup> and their dynamics<sup>7,8</sup> for a period of few picoseconds. In case of graphene nanostructures, the absence of dangling bonds in a DV is responsible for its formation energy being lower than that of two isolated SVs<sup>9-11</sup>. Also, the energetic stability of divacancy-defected graphene nanostructures is determined by the position of the DV<sup>12</sup>, size and edge termination type (zigzag or armchair) of the nanoflake<sup>13</sup>. The shape of the graphene nanoflakes with divacancies is also crucial in deciding the spin multiplicity of the ground state of these structures<sup>14</sup>.

Even though a considerable amount of literature is available on the microscopic imaging, identification of real-time dynamics of carbon vacancies and their energetics in graphene nanostructures, there is no report till date to highlight the variation in electronic and optical properties due to structural relaxation of DVs in SW-defected GQDs. In this work, we perform extensive electron-correlated computations based on the Pariser-Parr-Pople (PPP) model Hamiltonian and configuration-interaction (CI) methodology to systematically explore for the first time, the imprints of structural relaxation in modulating the electronic and optical properties of hydrogen-passivated GQDs having divacancy imperfections as well as armchair, zigzag and topologically SW-reconstructed zigzag (reczag) edge terminations. In order to compare and rationalize different computational approaches, we have also employed the TDDFT methodology to compute the absorption spectra of these systems. Our computed results demonstrate that structural relaxation, divacancy-position, and spin multiplicity are pivotal in determining the energetic ordering, decay channels for prompt as well as delayed fluorescence of tunable wavelengths and the marked optical absorption spectral features of singlet and triplet states.

# Theoretical model and computational approach

The divacancy defect is introduced at (i) the centre and (ii) the reczag edge of the GQD and their optimized structures are obtained by relaxing the configurations using the Gaussian 16 program package<sup>15</sup>, using a cc-pvdz basis set at restricted Hartree-Fock (RHF) level. The electron-correlated computations on these optimized structures are then initiated by applying our theoretical model based on Pariser-Parr-Pople (PPP) Hamiltonian<sup>16,17</sup> denoted by

$$\begin{aligned}
 H = & - \sum_{i,j,\sigma} t_{ij} \left( c_{i\sigma}^\dagger c_{j\sigma} + c_{j\sigma}^\dagger c_{i\sigma} \right) + U \sum_i n_{i\uparrow} n_{i\downarrow} \\
 & + \sum_{i<j} V_{ij} (n_i - 1)(n_j - 1)
 \end{aligned} \tag{1}$$

Here, the first term indicates the kinetic energy of the  $p_z$  electron having spin  $\sigma$ , when it delocalizes from the  $i^{th}$  carbon atom to its adjacent  $j^{th}$  carbon atom. The parameter  $t_{ij}$  represents the hopping matrix term between adjoining carbon atoms while  $c_{i\sigma}^\dagger$  ( $c_{i\sigma}$ ) creates (annihilates) the  $p_z$  electron at  $i^{th}$  location. The value of hopping matrix element,  $t_0$ , is selected as 2.4 eV when the bond length between adjacent carbon atoms,  $R_0$ , is 1.4 Å. In this work, the magnitude of hopping matrix elements corresponding to C-C bond lengths shorter or longer than 1.4 Å are derived from the relationship  $t_{ij} = t_0 e^{(R_0 - R_{ij})/\delta}$ , with  $\delta = 0.73$  Å<sup>18</sup>. The on-site Coulomb repulsion between the electrons is denoted by the second term in Eq. 1 wherein,  $n_i = \sum_\sigma c_{i\sigma}^\dagger c_{i\sigma}$  considers all electrons with spin  $\sigma$  on  $i^{th}$  carbon atom. The last term in this equation depicts long-range Coulomb repulsion with the parameter  $V_{ij}$  incorporating screening effects in accordance to the Ohno relationship<sup>19</sup>

$$V_{ij} = U / \kappa_{i,j} (1 + 0.6117 R_{i,j}^2)^{1/2} \tag{2}$$

wherein, the screening effects are simulated by the dielectric constant ( $\kappa_{i,j}$ ) of the system

and  $R_{i,j}$  denotes the spacing between adjacent carbon atoms (in Å). The screened parameters with  $U = 8.0$  eV,  $\kappa_{i,i} = 1.0$  and  $\kappa_{i,j} = 2.0$  ( $i \neq j$ ) are employed, in agreement with our earlier studies<sup>20–24</sup>.

For determining the singlet optical absorption spectra of our GQDs, electron correlated computations are performed by implementing the MRSDCI methodology. For this objective, a code developed by our group<sup>25</sup> is used to initially transform the PPP Hamiltonian from the site basis to molecular orbital (MO) basis by employing the MOs obtained from the mean-field RHF computations. This transformed hamiltonian and a single reference space comprising of RHF ground state are considered for calculating the preliminary CI matrix. The transition electric dipole matrix elements between different excited states, necessary for calculating the optical absorption spectra, are then derived from the eigenfunctions generated from this CI matrix. Thereafter, the excited states leading to peaks in the absorption profile are discerned and their corresponding reference eigenfunctions with coefficients above a predetermined convergence criterion are taken into consideration to create the new reference space for performing the next MRSDCI calculation. These steps are repeated in chronological order until convergence of the excitation energies and optical absorption spectra of the system are achieved within an acceptable tolerance. In order to make the computations attainable, a small number of initial low-energy occupied orbitals are frozen and upper high-energy virtual orbitals are deleted to reduce the set of active MOs.

The transition dipole components and excited state energies are employed to compute the Lorentzian line shaped ground state optical absorption cross-section  $\sigma(\omega)$  given by,

$$\sigma(\omega) = 4\pi\alpha \sum_i \frac{\omega_{i0} |\langle i | \hat{\mathbf{e}} \cdot \mathbf{r} | 0 \rangle|^2 \gamma}{(\omega_{i0} - \omega)^2 + \gamma^2}, \quad (3)$$

where,  $\omega$ ,  $\omega_{i0}$ ,  $\hat{\mathbf{e}}$ ,  $\mathbf{r}$ ,  $\alpha$  and  $\gamma$  represent the frequency of incident radiation, energy difference (in frequency units) between ground ( $|0\rangle$ ) and excited ( $|i\rangle$ ) levels, polarization direction of incident radiation, position operator, fine structure constant and absorption line-width, respectively.

For computing the triplet absorption spectrum, the same methodology is adopted by considering the many-electron wave-functions having triplet spin multiplicity and then deriving the corresponding transition dipole elements and excited triplet state energies.

For the purpose of authenticating our PPP-model-based configuration-interaction (PPP-CI) results, the optical absorption spectra of the optimized configurations (B3LYP/6-31g(d)) are computed by employing the TD-B3LYP approach using the Gaussian 16 program package<sup>15</sup>. This framework is adopted as it can accurately describe the ground and excited-state properties of medium to large-sized nanostructures at a low computational cost.

## Results and Discussion

### Structure and energetics

Figure (1a - 1b) displays the initial unrelaxed geometrical configuration of hydrogen-passivated GQDs with armchair, zigzag and reczag edges having divacancies at the centre (GQD-DV1) and at the reczag edge (GQD-DV2). The optimized geometries GQD-DV1-585 and GQD-DV2-594 obtained after structural relaxation of GQD-DV1 and GQD-DV2 systems are depicted in figs. 1c and 1d, respectively. Our results demonstrate that the geometry of the systems is altered significantly on relaxation. The divacancies at the centre reconstruct into a pattern composed of two pentagons and a central octagon while the DVs at the reczag edge transform into an arrangement consisting of a nonagon in between a pentagon and a tetragon. The bond-lengths between the adjacent carbon atoms are in the range (1.35 - 1.49) Å for the unrelaxed systems while they vary from 1.33 Å to 1.61 Å for the relaxed configurations. The coordinates of the carbon and hydrogen atoms in all these systems are listed in Table S1 of the Supporting Information<sup>26</sup>. A detailed analysis of the structural energetics of optimized GQD-DV1-585 and GQD-DV2-594 geometries (obtained from Gaussian 16 program package) reveals that they have equal energies, implying that their structural stability is independent of the position of divacancies.

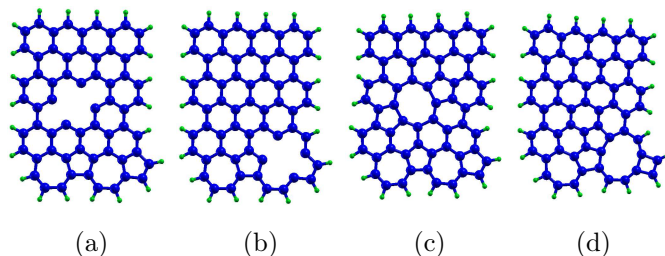


Figure 1: Schematic representation of (a) GQD-DV1, (b) GQD-DV2, (c) GQD-DV1-585, and (d) GQD-DV2-594 systems. The blue and green spheres denote carbon and hydrogen atoms, respectively.

## Energetic ordering and decay mechanism of triplet and singlet states

Figure 2 exhibits the energetic ordering of the first few singlet ( $S_m, m \geq 1$ ) and triplet ( $T_n, n \geq 0$ ) states of the relaxed systems considered in this work, computed using the PPP-CI methodology. Our investigations reveal that the lowest energy singlet state is below the first triplet state for the unrelaxed systems, while the trend is reversed for their relaxed counterparts. The energy difference between the first singlet ( $S_1$ ) and triplet ( $T_0$ ) states for GQD-DV1-585 and GQD-DV2-594 are 0.04 eV and 0.05 eV, respectively, implying that the high-spin triplet state will be the stable ground state of these systems at room temperature (0.025 eV). Hence, the high-spin ground state of these relaxed configurations having robust thermal stability at room temperature significantly enhances the potential application of these GQDs in the field of organic spintronic devices.

The low energy triplet excitons in the  $T_1$  level of GQD-DV1-585 and GQD-DV2-594 can promptly fluoresce to the  $T_0$  state emitting wavelengths (2897 nm) and (1044 nm), respectively, in the near-infrared (NIR) range. Alternately, the marginal energy splitting between the upper triplet and singlet excited levels facilitates the conversion of high-energy triplet excitons to the emissive singlet level ( $S_2$ ) via reverse intersystem crossing (RISC) process. The consequent radiative decay from  $S_2$  to  $S_1$  can give rise to delayed fluorescence, with long emission lifetime, in both these systems. In case of GQD-DV1-585, the small energy difference between  $S_2$  and  $T_1$  ( $\Delta E_{ST} = 0.027$  eV) as also between  $S_4$  and  $T_2$  ( $\Delta E_{ST} = 0.034$

eV) states can lead to delayed fluorescence (2966 nm) along the  $T_1 \rightarrow S_2 \rightarrow S_1$  and  $T_2 \rightarrow S_4 \rightarrow S_3 \rightarrow S_2 \rightarrow S_1$  channels, respectively. A transition involving high-lying excited energy levels ( $T_n \rightarrow S_m, n \geq 1, m \geq 2$ ) is termed as “hot exciton” process. In particular, the large energy separation between  $T_2$  and  $T_1$  (0.663 eV) states substantially enhances the possibility of RISC “hot exciton” process<sup>27</sup> in contrast to the internal conversion (IC) of triplet excitons along  $T_2 \rightarrow T_1$  route in this system. In case of GQD-DV2-594, the very small singlet-triplet energy splitting ( $\Delta E_{ST} = 0.057$  eV) between the  $S_3$  and  $T_1$  states can prompt delayed fluorescence (1272 nm) along the  $T_1 \rightarrow S_3 \rightarrow S_2 \rightarrow S_1$  decay path. Hence, our findings illustrate that introducing divacancies in SW-defected GQDs is an efficient mechanism for realizing both prompt as well as delayed fluorescence of varied wavelengths and the range of tunability of these wavelengths is more for GQD-DV2-594 as compared to GQD-DV1-585. In addition, the energetic proximity of the  $T_0$  and  $S_1$  energy levels can induce a spin cross-over of the ground state of these systems from triplet to singlet at elevated temperatures. However, even when these systems are in the singlet ground state, the marginal singlet-triplet energy splitting coupled with the large energy gaps between the triplet states can trigger delayed fluorescence via intersystem crossing and RISC processes along with normal luminescence. A schematic representation of this mechanism is illustrated in fig. 3. Hence, SW-defected GQDs with divacancy can be suitably utilized to enhance the efficiency of next-generation FOLED devices by harvesting both triplet and singlet excitons, simultaneously.

## Optical properties of divacancy and SW-defected GQDs

We now investigate the role of structural relaxation and electron-electron correlation in governing the optical spectral features of all the above considered divacancy and SW-defected GQDs. For this purpose, PPP-CI and TDDFT methodologies are adopted to compute and analyze the linear absorption spectra for both the spin multiplicity states, since it is feasible for these GQDs to exist in either of these states at high temperatures. The precision of our CI results, in the absence of experimental data, are validated by the large dimensions



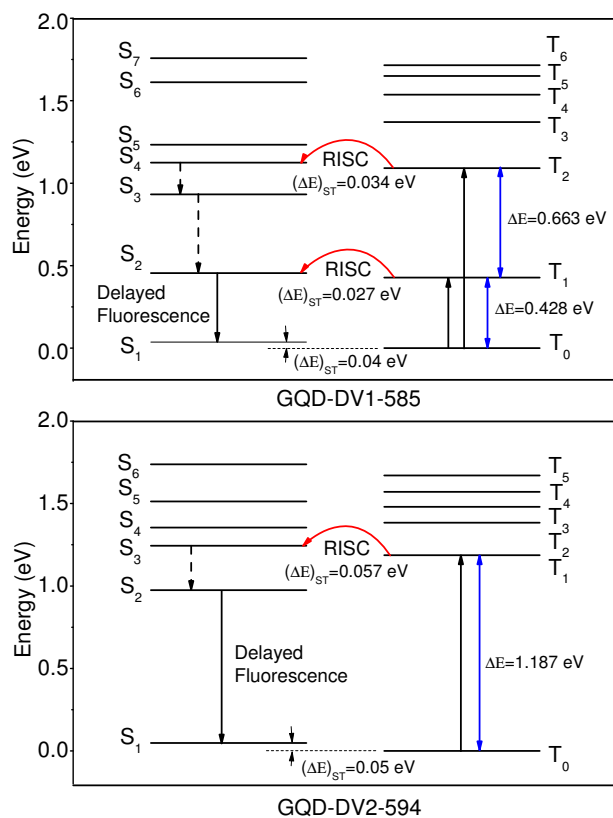


Figure 2: Energetic ordering of the first few singlet and triplet states of GQD-DV1-585 and GQD-DV2-594 computed by adopting PPP-CI approach.

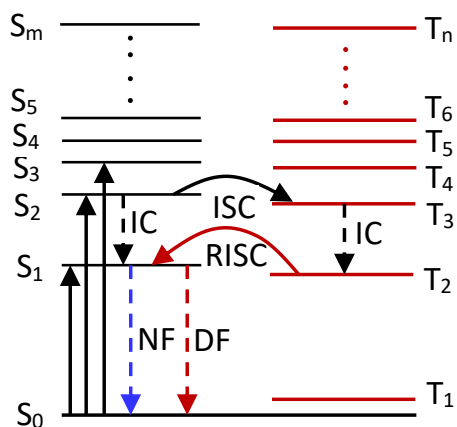
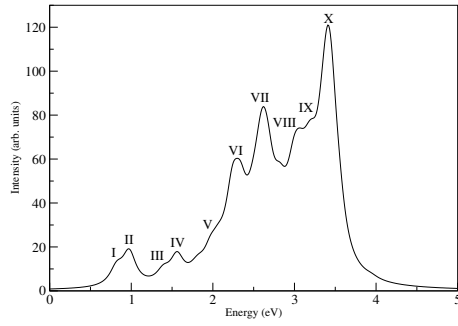


Figure 3: Schematic representation of prompt or normal fluorescence (NF), delayed fluorescence (DF), internal conversion (IC), intersystem crossing (ISC) and reverse intersystem crossing (RISC) processes occurring when divacancy and SW-defected GQDs are in the singlet ground state.

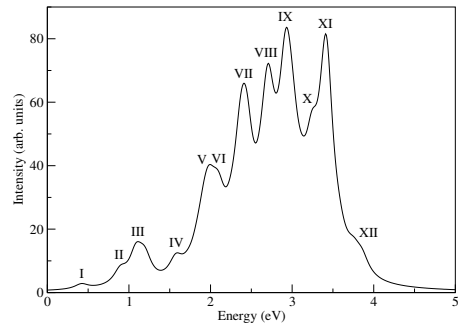
(>  $10^6$ ) of the diagonalized CI matrices (Table S2<sup>26</sup>).

A detailed investigation of the PPP-CI singlet absorption spectra (Figs. 4(a-d)) and quantitative data of the corresponding excited states (Tables S3-S6<sup>26</sup>) reveals the following characteristics: (i) The first peaks of the unrelaxed structures GQD-DV1 and GQD-DV2, are strongly dominated by transition of a single electron from H to L+1 level, denoted by  $|H \rightarrow L + 1\rangle$ , henceforth. However, when the SW-defected GQDs with DV undergo relaxation, the first peak of GQD-DV2-594 is primarily due to double excitation  $|H \rightarrow L; H \rightarrow L\rangle$ , while for the case of GQD-DV1-585, this peak is mainly composed of the single excitation  $|H \rightarrow L + 1\rangle$ , along with substantial contribution from the doubly excited wave-function  $|H \rightarrow L; H \rightarrow L + 1\rangle$ . (ii) The singly-excited electronic configuration  $|H \rightarrow L\rangle$  is primarily responsible for the second absorption peak of GQD-DV1, GQD-DV1-585 and GQD-DV2. However, in case of GQD-DV2-594, this excitation leads to an extremely small hump at energy 0.93 eV, which is hardly perceptible in the optical absorption spectrum. These results are primarily a consequence of electron-electron correlations coupled with broken particle-hole symmetry due to DV and SW-type imperfections in these GQDs. (iii) The second peak of GQD-DV1 and GQD-DV2, dominantly due to  $|H \rightarrow L\rangle$  transition, has mixed  $x - y$  polarization with higher magnitude of the transition dipole moment along the y axis, while this peak gets predominantly x-polarized for GQD-DV1-585. (iv) The position of the most intense (MI) peak is in the UV range for GQD-DV1 while it shifts to the violet range for its relaxed configuration. This is in stark contrast to the reverse trend demonstrated by SW-defected GQDs having divacancies at the reczag edge, wherein the MI peak shifts from violet to UV range on relaxation. In addition, the magnitudes of these red/blue-shifts are quite comparable to each other. (v) The strength of the most intense peak of GQD-DV1 decreases significantly after relaxation, while no such trend is observed for GQD-DV2. (vi) The optical absorption peak profile (peak pattern as well as peak intensity) is drastically altered when the DV-defected GQDs undergo relaxation.

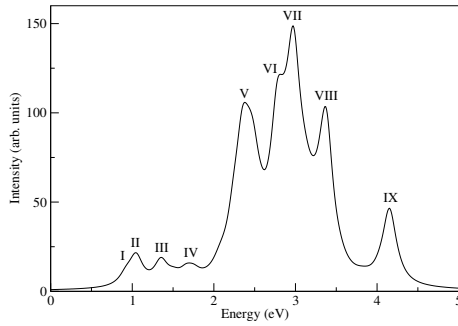
In case of the computed PPP-CI triplet one-photon absorption spectra, the peak positions



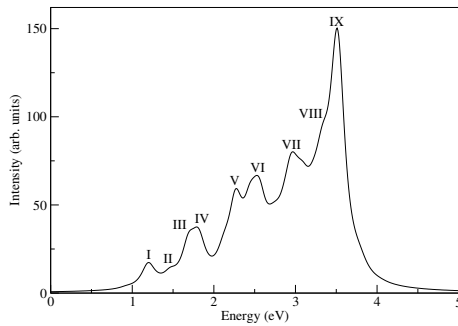
(a)



(b)



(c)



(d)

Figure 4: Singlet optical absorption spectra of (a) GQD-DV1, (b) GQD-DV1-585, (c) GQD-DV2 and (d) GQD-DV2-594 calculated by adopting the PPP-CI approach. These spectra are broadened with a uniform line width of 0.1 eV.

represent the excitation energies of the higher triplet states with respect to the lowest triplet state. A detailed examination of this spectra (Figs. 5(a-d)) and quantitative data of the corresponding excited states (Tables S7-S10<sup>26</sup>) elucidates the following features: (i) The entire triplet spectrum of GQD-DV1, GQD-DV1-585 and GQD-DV2 is red-shifted while that of GQD-DV2-594 is marginally blue-shifted with respect to their corresponding singlet spectrum. However, the MI peak of the triplet absorption spectrum is always red-shifted compared to its singlet counterpart. (ii) The MI peak is red/blue-shifted when SW-defected GQDs with DV imperfections at the centre/reczag edge undergo relaxation, in agreement with the behaviour exhibited by their corresponding singlet spectra. The MI peak is in the green band for both the unrelaxed and relaxed SW-defected GQDs with DVs at the core. However, the position of MI peak is shifted from blue to violet range when GQD-DV2 relaxes to GQD-DV2-594 configuration. The magnitude of the computed blue-shift (0.45 eV) is much higher compared to the red-shift (0.14 eV) for the triplet spectra of these GQDs. This trend is distinctly different from the comparable values of the red and blue-shift (0.47 and 0.54 eV, respectively) of the singlet MI peak. (iii) The intensity of the strongest triplet absorption peak is always less/more than its singlet counterpart for both relaxed and unrelaxed SW-defected GQDs with DV imperfections at the centre/reczag edge. Further, the strength of the triplet MI peak always reduces when GQD-DV1 and GQD-DV2 systems are relaxed, with the reduction being more evident for GQD-DV1 geometry. (iv) The number of absorption peaks in the IR and UV band is always less in the triplet spectra compared to their corresponding singlet spectra for all our studied GQDs. However, the number of triplet optical peaks in the visible energy range increases for GQD-DV1, GQD-DV2 and GQD-DV2-594, while it is equal to the number of singlet peaks in this energy domain for GQD-DV1-584 configuration. (v) The number of triplet excited states with major contributions from double excitations or having significant mixing of many singly excited configurations is more than the number of singlet excited states with such attributes. This emphasizes that the strength of electron-electron correlations is greater for triplet manifold in comparison to singlet states.

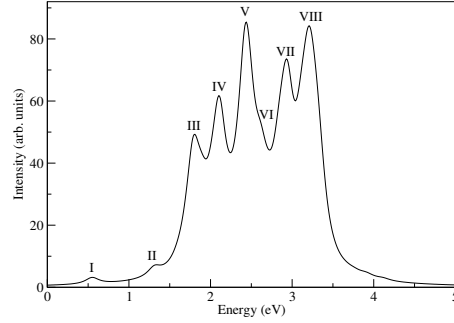
A comparison of the MI peak energies of the singlet absorption spectra of GQD-DV1-585 and GQD-DV2-594, obtained from TDDFT and PPP-CI approaches (Table 1), reveal that the TDDFT values are in excellent agreement with the PPP-CI results. In contrast, there is a large discrepancy between the MI peak energies of the triplet absorption spectra, computed from TDDFT and PPP-CI methodologies, with the variation being more pronounced for GQD-DV2-594. This deviation is due to the fact that TDDFT which is analogous to CI-singles (CIS) methodology considers only single particle-hole excitations and therefore, cannot accurately describe the triplet states where electron correlation effects are highly dominant. In addition, the TDDFT values of the MI peak of the triplet absorption spectrum is always red-shifted compared to its singlet counterpart, in agreement with the PPP-CI results. Hence, our computations demonstrate that the PPP-CI approach is more effective than TDDFT methodology in predicting the trends of the singlet and triplet absorption spectrum of these defected systems.

Table 1: Comparison of MI peak energies of the singlet and triplet absorption spectra of GQD-DV1-585 and GQD-DV2-594, obtained from TDDFT and PPP-CI approaches.

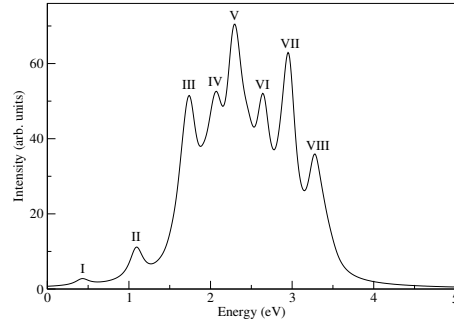
System	MI peak energy (eV)			
	Singlet Absorption Spectrum		Triplet Absorption Spectrum	
	TDDFT	PPP-CI	TDDFT	PPP-CI
GQD-DV1-585	3.01	2.93	2.66	2.28
GQD-DV2-594	3.53	3.52	2.56	3.09, 3.12

## Conclusions

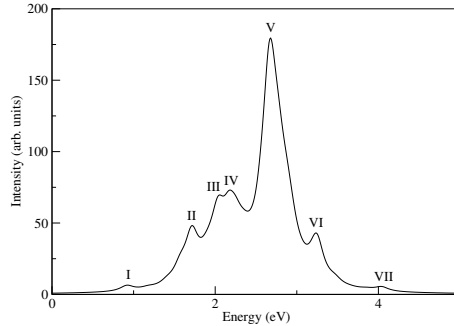
In summary, we have successfully captured the signatures of structural relaxation in governing the electronic and optical properties of SW-defected GQDs with divacancy by performing extensive electron-correlated computations based on the PPP Hamiltonian and TDDFT approach. It is observed that the geometry of the relaxed systems is critically dependent on the position of the divacancy in these structures. Our results conclusively show that structural relaxation switches the electronic ground-state configuration of these systems from low-spin



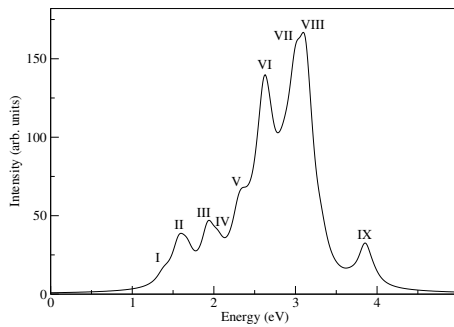
(a)



(b)



(c)



(d)

Figure 5: Triplet optical absorption spectra of (a) GQD-DV1, (b) GQD-DV1-585, (c) GQD-DV2 and (d) GQD-DV2-594 calculated by adopting the PPP-CI approach. These spectra are broadened with a uniform line width of 0.1 eV. The peak positions represent the excitation energies of the higher triplet states with respect to the lowest triplet state.

singlet to high-spin triplet state. The thermal stability of this high-spin triplet ground state of the relaxed systems at and above the room temperature significantly augments the applicability of these materials in designing spintronic devices. Notably, our computations reveal that the energetic ordering of the singlet and triplet states of the relaxed systems facilitates the possibility of achieving both prompt as well as delayed fluorescence of different wavelengths and the tunability range of the emission wavelengths is determined by the position of divacancy in these SW-defected GQDs. Our findings signify that the entire singlet and triplet optical absorption profile (peak pattern as well as intensity) is substantially altered due to structural relaxation. Specifically, the nature of shift exhibited by the most intense absorption peak of the relaxed GQDs with respect to their unrelaxed counterpart depends on the location of the divacancy. The magnitude of this shift is determined by the spin multiplicity of the energy states. The spin multiplicity also has distinct imprints on the entire absorption peak profile of these systems. Also, all these marked features of the optical absorption spectrum can be more accurately described by the PPP-CI methodology as compared to the TDDFT approach. In conclusion, our results provide new insights to the novel concept of exploiting SW-defected GQDs with divacancy for designing highly efficient optoelectronic and spintronic devices.

## Supporting Information Available

The coordinates of the carbon and hydrogen atoms, dimensions of CI matrices considered for computing the linear optical absorption spectra of singlet and triplet spin multiplicity of GQD-DV1, GQD-DV1-585, GQD-DV2 and GQD-DV2-594 systems, energies, transition dipole moments and the configurations contributing dominantly to the many-particle wave functions of the excited states primarily responsible for the absorption peaks in the PPP-CI singlet and triplet spectra of GQD-DV1, GQD-DV1-585, GQD-DV2 and GQD-DV2-594 configurations are included in the supporting information.

## References

- (1) Hirata, S. Recent Advances in Materials with Room-Temperature Phosphorescence: Photophysics for Triplet Exciton Stabilization. *Advanced Optical Materials* **2017**, *5*, 1700116.
- (2) Hashimoto, A.; Suenaga, K.; Gloter, A.; Urita, K.; Iijima, S. Direct evidence for atomic defects in graphene layers. *Nature* **2004**, *430*, 870.
- (3) Meyer, J. C.; Kisielowski, C.; Erni, R.; Rossell, M. D.; Crommie, M. F.; Zettl, A. Direct Imaging of Lattice Atoms and Topological Defects in Graphene Membranes. *Nano Letters* **2008**, *8*, 3582–3586.
- (4) Cretu, O.; Krasheninnikov, A. V.; Rodriguez-Manzo, J. A.; Sun, L.; Nieminen, R. M.; Banhart, F. Migration and Localization of Metal Atoms on Strained Graphene. *Phys. Rev. Lett.* **2010**, *105*, 196102.
- (5) Girit, C. O.; Meyer, J. C.; Erni, R.; Rossell, M. D.; Kisielowski, C.; Yang, L.; Park, C.-H.; Crommie, M. F.; Cohen, M. L.; Louie, S. G.; Zettl, A. Graphene at the Edge: Stability and Dynamics. *Science* **2009**, *323*, 1705–1708.
- (6) Kim, Y.; Ihm, J.; Yoon, E.; Lee, G.-D. Dynamics and stability of divacancy defects in graphene. *Phys. Rev. B* **2011**, *84*, 075445.
- (7) Lee, G.-D.; Wang, C. Z.; Yoon, E.; Hwang, N.-M.; Kim, D.-Y.; Ho, K. M. Diffusion, Coalescence, and Reconstruction of Vacancy Defects in Graphene Layers. *Phys. Rev. Lett.* **2005**, *95*, 205501.
- (8) Leyssale, J.-M.; Vignoles, G. L. A Large-Scale Molecular Dynamics Study of the Divacancy Defect in Graphene. *The Journal of Physical Chemistry C* **2014**, *118*, 8200–8216.
- (9) Krasheninnikov, A.; Lehtinen, P.; Foster, A.; Nieminen, R. Bending the rules: Con-



- trasting vacancy energetics and migration in graphite and carbon nanotubes. *Chemical Physics Letters* **2006**, *418*, 132–136.
- (10) Kotakoski, J.; Krasheninnikov, A. V.; Nordlund, K. Energetics, structure, and long-range interaction of vacancy-type defects in carbon nanotubes: Atomistic simulations. *Phys. Rev. B* **2006**, *74*, 245420.
- (11) El-Barbary, A. A.; Telling, R. H.; Ewels, C. P.; Heggie, M. I.; Briddon, P. R. Structure and energetics of the vacancy in graphite. *Phys. Rev. B* **2003**, *68*, 144107.
- (12) Sahan, Z.; Berber, S. Divacancy in graphene nano-ribbons. *Physica E: Low-dimensional Systems and Nanostructures* **2019**, *106*, 239–249.
- (13) Liu, L.; Chen, S. Geometries and Electronic States of Divacancy Defect in Finite-Size Hexagonal Graphene Flakes. *Journal of Chemistry* **2017**, *2017*, 8491264.
- (14) Yumura, T.; Awano, T.; Kobayashi, H.; Yamabe, T. Platinum Clusters on Vacancy-Type Defects of Nanometer-Sized Graphene Patches. *Molecules* **2012**, *17*, 7941–7960.
- (15) Frisch, M. J.; Trucks, G. W.; Schlegel, H. B.; Scuseria, G. E.; Robb, M. A.; Cheeseman, J. R.; Scalmani, G.; Barone, V.; Petersson, G. A.; Nakatsuji, H.; et al., Gaussian 16 Revision C.01. 2016; Gaussian Inc. Wallingford CT.
- (16) Pople, J. A. Electron interaction in unsaturated hydrocarbons. *Trans. Faraday Soc.* **1953**, *49*, 1375–1385.
- (17) Pariser, R.; Parr, R. G. A SemiEmpirical Theory of the Electronic Spectra and Electronic Structure of Complex Unsaturated Molecules. II. *J. Chem. Phys.* **1953**, *21*, 767–776.
- (18) Basak, T.; Basak, T.; Shukla, A. Graphene quantum dots with a Stone-Wales defect as a topologically tunable platform for visible-light harvesting. *Phys. Rev. B* **2021**, *103*, 235420.

- (19) Ohno, K. Some remarks on the Pariser-Parr-Pople method. *Theoretica chimica acta* **1964**, *2*, 219–227.
- (20) Basak, T.; Basak, T.; Shukla, A. Electron correlation effects and two-photon absorption in diamond-shaped graphene quantum dots. *Phys. Rev. B* **2018**, *98*, 035401.
- (21) Basak, T.; Shukla, A. Optical signatures of electric-field-driven magnetic phase transitions in graphene quantum dots. *Phys. Rev. B* **2016**, *93*, 235432.
- (22) Basak, T.; Chakraborty, H.; Shukla, A. Theory of linear optical absorption in diamond-shaped graphene quantum dots. *Phys. Rev. B* **2015**, *92*, 205404.
- (23) Basak, T.; Basak, T. Electro-absorption spectra of magnetic states of diamond shaped graphene quantum dots. *Materials Today: Proceedings* **2020**, *26*, 2058 – 2061, 10th International Conference of Materials Processing and Characterization.
- (24) Basak, T.; Basak, T. Characterization of magnetic states of graphene quantum dots of different shapes by application of electric field. *Materials Today: Proceedings* **2020**, *26*, 2069 – 2072, 10th International Conference of Materials Processing and Characterization.
- (25) Sony, P.; Shukla, A. A general purpose Fortran 90 electronic structure program for conjugated systems using Pariser-Parr-Pople model. *Computer Physics Communications* **2010**, *181*, 821 – 830.
- (26) Supporting Information.
- (27) Hu, D.; Yao, L.; Yang, B.; Ma, Y. Reverse intersystem crossing from upper triplet levels to excited singlet: a hot excitation path for organic light-emitting diodes. *Philosophical Transactions of the Royal Society A: Mathematical, Physical and Engineering Sciences* **2015**, *373*, 20140318.

# Graphical TOC Entry

